JBIC (1999) 4:478–494

ORIGINAL ARTICLE

Pedro M. Matias · Lígia M. Saraiva
Cláudio M. Soares · Ana V. Coelho · Jean LeGall
Maria Arménia Carrondo

Nine-haem cytochrome *c* from *Desulfovibrio desulfuricans* ATCC 27774: primary sequence determination, crystallographic refinement at 1.8 and modelling studies of its interaction with the tetrahaem cytochrome c_3

Received: 15 March 1999 / Accepted: 19 May 1999

Abstract A monomeric nine-haem cytochrome *c* (9Hcc) with 292 amino acid residues was isolated from cells of the sulfate- and nitrate-reducing bacterium *Desulfovibrio desulfuricans* ATCC 27774 grown under both nitrate- and sulfate-respiring conditions. The nucleotide sequence encoding the 292 residues was determined, allowing the correction of about 10% of the previous primary structure, determined from 1.8 Å electron density maps. The refinement at 1.8 Å resolution of the structural model was completed, giving an *R*-value of 16.5%. The nine haem groups are arranged into two tetrahaem clusters, located at both ends of the molecule, with Fe-Fe distances and local protein fold very similar to tetrahaem cytochromes c_3, and the extra haem is located asymmetrically between the two regions. The new primary sequence determination confirmed the 39% sequence homology found between this cytochrome and the C-terminal region (residues 229–514) of the high-molecular-weight cytochrome *c* (Hmc) from *D. vulgaris* Hildenborough, providing strong evidence of structural similarity between 9Hcc and the C-terminal region of Hmc. The interaction between 9Hcc and the tetrahaem cytochrome c_3 from the same organism was studied by modelling methods, and the results suggest that a specific interaction is possible between haem 4 of tetrahaem cytochrome c_3 and haem 1 or haem 2 of 9Hcc, in agreement with previous kinetic experiments which showed the catalytic effect of the tetrahaem cytochrome c_3 upon the reduction of 9Hcc by the [NiFe] hydrogenase from *D. desulfuricans* ATCC 27774. These studies suggest a role for 9Hcc as part of the assembly of redox proteins involved in recycling the molecular hydrogen released by the cell as a result of substrate oxidation.

Key words Nine-haem cytochrome *c* · Multiple wavelength anomalous dispersion phasing method · Sulfate-reducing bacteria · Electron transfer · Modelling and interaction studies

P.M. Matias · L.M. Saraiva · C.M. Soares · A.V. Coelho
J. LeGall · M.A. Carrondo (✉)
Instituto de Tecnologia Química e Biológica, Universidade Nova de Lisboa, Apartado 127, P-2780 Oeiras, Portugal
e-mail: carrondo@itqb.unl.pt
Tel.: +351-1-4418215
Fax: +351-1-4411277

A.V. Coelho
Chemistry Department, Universidade de Évora, P-7000 Évora Portugal

J. LeGall
Department of Biochemistry and Molecular Biology
University of Georgia, Athens, GA 30602 USA

Introduction

The best characterized of the multi-haem cytochromes *c* found in sulfate-reducing bacteria (SRBs) is the tetrahaem cytochrome c_3, which forms a specific interaction with hydrogenase [1]: when coupled to the oxidation of molecular hydrogen, catalysed by this enzyme, it is capable of transferring two electrons and two protons in a concerted step through a mechanism described as a "proton thruster" [2]. Other, even more complex, cytochromes *c* (for a review, see [3]) are found in SRBs belonging to the genus *Desulfovibrio* and related organisms, but so far very little is known concerning their structures and their relationships with the ubiquitous tetrahaem cytochrome c_3. The nine-haem cytochrome *c* (9Hcc), isolated from cells of the sulfate- and nitrate-reducing bacterium *Desulfovibrio desulfuricans* ATCC 27774 (Dd 27774) [4], is one of these molecules. Very similar amounts of the protein were obtained from cells grown either in sulfate- or nitrate-respiring conditions, indicating that this cytochrome is constitutively synthesized under both growing conditions and therefore very likely an important electron carrier in both systems [4, 5]. Its primary and three-dimensional structures were previously determined using the multiple wavelength anomalous dispersion (MAD) phasing method and re-

fined against 1.8 Å diffraction data [6]. The model contains 292 residues plus nine haem groups.

Kinetic experiments showed that 9Hcc can be reduced by the [NiFe] hydrogenase from *D. desulfuricans* ATCC 27774, and that this reduction is faster in the presence of the tetrahaem cytochrome c_3 from the same organism [6]. This behaviour is similar to that found between the [NiFe] hydrogenase and the high-molecular-weight cytochrome *c* (Hmc) in *D. vulgaris* Hildenborough [7]. Furthermore, a 39% sequence identity was found between 9Hcc and the C-terminal region (residues 229–514) of Hmc, providing strong evidence of structural similarity between 9Hcc and the C-terminal region of Hmc [6]. This led to the proposal that 9Hcc takes the role of Hmc in *D. desulfuricans* ATCC 27774 and is part of the assembly of redox proteins involved in recycling the molecular hydrogen released by the cell as a result of substrate oxidation. 9Hcc has also been proposed to be involved in electron transfer across the cytoplasmic membrane [6]. Although a mechanism for the interaction between [NiFe] hydrogenase, 9Hcc and the tetrahaem cytochrome c_3 in Dd 27774 has not yet been established, the kinetics do suggest that the interaction between 9Hcc and the tetrahaem cytochromec_3 is likely to play an important role therein. To study the interaction between 9Hcc and the tetrahaem cytochrome c_3 from *D. desulfuricans* ATCC 27774 by molecular modelling methods, correct sequence information is essential, in particular the distinction between asparagine and aspartic acid residues, and glutamine and glutamic acid residues, which have very different electrostatic properties and could not be distinguished solely on the basis of their electron density at 1.8 Å. This is particularly important for residues located on the molecular surface and, as such, likely to play a role in the shaping of the electrostatic field guiding the interaction between two redox proteins.

In this study we report the nucleotide sequence and the deduced amino acid sequence of the 292 residues of the 9Hcc structural model, the refinement of the corrected model at 1.8 Å resolution and the analysis of the interaction between 9Hcc and the tetrahaem cytochrome c_3 from *D. desulfuricans* ATCC 27774 by molecular modelling methods.

Materials and methods

Molecular biology

D. desulfuricans ATCC 27774 was grown as previously described [8] and its genomic DNA isolated [9] and used in the subsequent polymerase chain reactions (PCRs). Based on both extremities of the amino acid sequence corresponding to the N- and C-termini of the protein as previously determined from 1.8 Å electron density maps [6], two degenerate oligonucleotide primers (from Life Science Technologies) were designed: GCV GCV CTB GAR CCS ACS GAY WS and BGC BGC BGC CTT RTG RCA SGT SGT RC. The PCR cycling conditions were: 1 cycle at 94 °C for 3 min followed by 35 cycles at 94 °C for 45 s, 65 °C for 1 min, 72 °C for 1 min and a final extension at 72 °C for 7 min. The reaction product with 876 base pairs was purified by electrophoresis in a 1% Nusieve GTG agarose (FMC Bioproducts), filling in with Klenow (Amersham), ligated with T4 ligase (Boehringer Mannheim) into EcoRV cut pBluescript SK(+/–) vector and transformed into competent cells of *Escherichia coli* XL-1 Blue. Several plasmids containing the 876 base pairs product were purified with Qiagen Plasmid Purification kit and sequenced using the Cycle Sequencing Ready Reaction kit according to the supplier's instructions (Perkin Elmer). Double-stranded DNA sequencing was carried out in an Applied Biosystems 373A DNA Sequencer. Both strands of DNA from three plasmid preparations of clones were sequenced using primers complementary to part of the original sequence as well as T7, T3 and M13 forward and reverse primers.

Crystallographic refinement

The sequence of the previously refined structural model [6] was corrected with the program TURBO-FRODO [10], using the determined amino acid sequence and both the density-modified 2.4 Å as well as the final 1.8 Å electron density maps from the previous refinement. As the number of differences was small, the refinement of the corrected model was continued on F_o^2 with SHELXL [11] using all 91,192 independent reflections. The solvent model was corrected according to the criteria that new water molecules to be included should be visible as peaks higher than 3σ in the F_o-F_c electron density map, as peaks higher than 1σ in the $2F_o-F_c$ map, and should have distances to suitable donors or acceptors of hydrogen bonds between 2.4 and 3.2 Å. In addition, the occupation factors of all solvent oxygen atoms whose isotropic thermal motion parameter became higher than 50 Å^2 were arbitrarily set to 1/2. Solvent molecules for which the occupation factor of the oxygen atom was already 1/2 but whose isotropic thermal motion parameter nonetheless became higher than 50 Å^2 were rejected from the model. Anisotropic thermal motion parameters were refined for all the Fe and S atoms in the model, and an overall anisotropic scaling procedure between F_o and F_c was used. In the final cycles of refinement, all non-acidic hydrogen atoms were included in calculated positions and refined according to the riding model. This refinement converged to $R=16.5\%$. The final model includes some two-fold disordered regions: Ser58 (0.61), Ile74 (0.60), Val172 (0.57), Glu206 (0.54) and Ser243 (0.58) in molecule A; Ile117 to Pro120 (0.55), Glu191 (0.51) and Glu206 (0.63) in molecule B (values in parentheses represent the refined occupation factor of the major component). Also, two pairs of water molecules were refined according to a twofold disorder model. The final refinement statistics are presented in Table 1. The coordinates of the refined 9Hcc model have been deposited in the Protein Data Bank [12, 13] with accession code 2c9h.

Electron transfer calculations

Electron transfer in proteins is the subject of intense research (see [14, 15] for reviews). Rates of non-adiabatic electron transfer can be expressed as

$$k_{ET}=\frac{2\pi}{\hbar}[T_{DA}]^2(FC) \quad (1)$$

The term FC (Frank-Condon) contains the free energy dependence (reorganization and reaction free energy) of the electron transfer. The term T_{DA} describes the donor-acceptor interaction associated with electron tunnelling. The Frank-Condon factor is difficult to evaluate since it requires the knowledge of reorganization energies. However, it should be approximately constant for different complex conformations of the same partners. The term T_{DA} can be estimated using what has been commonly known as the Pathways model [16, 17], which models electron tunnelling through organized matter and has been applied successfully to a variety of electron transfer processes in proteins [15, 16, 18, 19].

Table 1 Final refinement statistics for 9Hcc

Resolution limits (Å)		24.0–1.80
Final *R*-factor (%) (all 91,192 reflections)		16.5
Nr. non-hydrogen protein atoms[a]		5,194
Nr. non-hydrogen protein atoms with zero occupancy		113
Nr. non-hydrogen protein atoms in disordered residues[b]		65
Nr. acetate ions/atoms		5 20
Nr. solvent molecules with full occupancy		707
Nr. solvent molecules with 1/2 occupancy		188
Nr. solvent molecules with disorder		4
Nr. least-squares parameters		25,099
Nr. restraints in final least-squares cycle		24,874
Disagreeable restraints ($\Delta > 3\sigma$)[c]		
BUMB, DANG, FLAT, SIMU		8, 4, 14, 4
Estimated overall r.m.s. coordinate error (Å)[d]		0.05
model r.m.s. deviations from ideality[c]		
Bond distances (Å)		0.011
Angle (1–3) distances (Å)		0.024
Average *B*-values (Å^2)[e]	9Hcc A	9Hcc B
Main-chain protein	17.5	20.7
Side-chain protein	21.6	24.6
Haem groups	13.8	18.2
Solvent (including acetate ions)	29.3	
Numbering scheme	9Hcc A	9Hcc B
Protein chain[f]	1A...292A	1B...292B
Haem groups	301A...309A	301B...309B
Acetate ions	1X...5X	
Solvent molecules[g]	1W...897W	

[a] Excluding atoms in the minor component of disordered regions
[b] Atoms in the minor disorder component
[c] Restraints defined according to SHELXL [11]
[d] Calculated with SIGMAA [37, 38]
[e] For the disordered residues, only the major component atoms were considered
[f] In the text, residue numbers without chain suffix refer to the same residue in both molecules
[g] In the text we use W1...W897 instead

In the present work, electron transfer calculations were performed using the program GREENPATH [20] that implements the Pathways model. These calculations and all others to be described below were done using molecule A from the crystallographic refinement.

Protein-protein interactions

The interaction between 9Hcc and the tetrahaem cytochrome c_3 was studied using Autodock 2.4 [21]. In this calculation we used the refined coordinates of 9Hcc and our previously refined model of tetrahaem cytochrome c_3 [22]. This methodology has been used before to study other electron transfer protein complexes [23]. Autodock uses the large molecule (in this case 9Hcc) to generate three-dimensional affinity grids for several relevant terms of molecular interaction. Grids are generated for van der Waals terms (one for each CNOSH atom type), hydrogen bonding and electrostatic interactions. Electrostatic screening by the solvent was modelled using a distance-dependent dielectric function [24]. These affinity grids cover the large molecule and an amount of space around it that is sufficiently large to fit the small molecule in any orientation. Grids of $140 \times 140 \times 140$ grid points and with distances between grid points of 1.2 Å were used. The small molecule (in this case, tetrahaem cytochrome c_3) is then placed at random positions within the grids and association solutions with low energy are searched using Monte Carlo simulated annealing in translation and rotation coordinate space. The large molecule is considered to be rigid by its representation as affinity grids. Despite the possibility of using internal flexibility in the small molecule, such a procedure was not used here, since it introduces too many degrees of freedom that cannot be efficiently searched. The simulated annealing procedure is optimized to sample the conformational space of interaction solutions and generate low energy associations. Each run consisted of 100 cycles of Monte Carlo at progressively lower temperature. Each cycle consists of a maximum of 20,000 accepted or rejected steps. The temperature of the first cycle is chosen to allow a large acceptance to rejection ratio. In Autodock this temperature will depend on the system and on the number of degrees of freedom involved. For this case the value of $RT = 126$ kJ/mol (R = perfect gas constant) worked well. For each cycle, a factor of 0.95 was used to reduce the temperature. This allows a slow annealing phase and a low acceptance to rejection ratio in the end. The initial maximum translation step was 1.0 Å and the maximum quaternion rotation step was 30°. The reduction factors of 0.9702 and 0.9770 were used per cycle for maximum translation and rotations steps, respectively; this resulted in 0.05 Å maximum translation steps and 3° maximum rotation steps in the last cycle. Two hundred runs were performed to obtain interaction solutions. The final structures were compared and clustered on the basis of their r.m.s. deviation, using a tolerance of 1.0 Å.

The GROMOS charge set for polar and aromatic hydrogen atoms [25, 26] was used to set the charges in the structures used in docking. Hydrogen atoms were positioned using GROMOS [25]. Then, the proton positions were optimized in vacuo using energy minimization, while keeping all heteroatoms rigid by the use of large [10,000 kJ/(mol nm)] positional restraints. The minimization consisted of 1000 steps of steepest descent. Since both proteins were crystallized at low pH, there are a number of propionates with abnormal protonation. Nevertheless, some of these abnormal protonations can be physiological. In this study we decided to use the protonation behaviour as observed in the structure for all cases where this protonation is evident. In the case of 9Hcc the propionates A from haem 4 and D from haem 5 were found to be protonated. In the case of tetrahaem cytochrome c_3, the propionate D from haem 4 was considered protonated as indicated by previous pK_a calculations [27]. The iron atom in the haem groups was assumed to be in the fully oxidized state, Fe(III), as in the crystallographic structures. The partial charges used for the haem groups were the same as previously described [27].

Molecular dynamics refinement of the best rigid solutions

To simulate the close association of the two molecules when placed into contact, we refined the initial structures of selected complexes using molecular dynamics simulations. The dynamics were calculated in vacuo using the same distance-dependent electrostatic function of Mehler and Solmajer [24] in Autodock. To avoid large changes in the two proteins owing to the absence of water, we used distance restraints to hold the C^α topology close to the experimentally derived structures. This was done for all C^α atoms in the structure and the constraints were implemented using soft harmonic potentials with force constants of 100 kJ/(mol nm). The GROMOS force field using aromatic and polar hydrogen atoms [25, 26] with improved *c*-type haem charges [27] was used in all simulations. The GROMOS 87 [25] package with modified versions of PROEM and PROMD for distance dependent electrostatics was used to perform the simulations. The twin range cutoff method [28] was used for electrostatic interactions with radius 8 Å and 14 Å, respectively. SHAKE [29] was applied for all bonds. A 0.002 ps step was used for the integration of the equations of motion. The refinement protocol consisted initially of 1000 steps of steepest descent minimization followed by 1000 steps of conjugated gradient minimization. A molecular dynamics simulation was started with initialization of atomic velocities from a distribution at 50 K. Then 20 ps of slow heating from 50 K to 300 K were calculated, followed by 200 ps of relaxation run at 300 K. Finally, slow cooling from 300 K to 0 K was done during 20 ps, followed by 1000 steps of conjugated gradient minimization.

Results and discussion

Primary sequence determination and comparison with previous sequence data

The DNA sequence obtained for the 876 base pairs coding for residues 1–292 of 9Hcc is shown in Fig. 1, along with the corresponding protein amino-acid sequence. The differences from the previously determined sequence from 1.8 Å electron density maps are also indicated on Fig. 1 as well as the haem group binding regions and second axial histidine ligands. A total of 26 sequence corrections were made, and can be divided into two kinds: for 12 residues, the amino acid assigned from the electron density maps had a shorter side chain than that of the correct amino acid. In our previous publication, it had already been recognized that some of these residues were probably incorrect (see fig. 1 in [6]); seven out of eight such noted residues were in fact wrongly assigned. The remaining five correspond to situations where the electron density maps were less clear in suggesting the possibility of a different (longer) side chain assignment. The remaining 14 residue corrections mainly consist of Asp/Asn and Glu/Gln ambiguity resolution, since asparagine cannot usually be distinguished from aspartic acid, and likewise for glutamine and glutamic acid. However, it was also found that two residues initially assigned as threonines were in fact valine residues. In this particular case it was found that, in each residue, one short van der Waals contact between a main chain carbonyl oxygen and a hydrogen from a methyl group from the valine side chain was mistaken for a hydrogen bond. Since only 253 of the 292 residues in 9Hcc were truly unknown, and as such assigned from 1.8 Å electron density maps, it can be said that only 10% of the sequence determined from the X-ray data was in error. These new results confirm the sequence identity previously reported between 9Hcc and the C-terminal region (residues 229–514) of the high-molecular-weight cytochrome *c* (Hmc) from *D. vulgaris* Hildenborough [6].

Fig. 1 Gene product and amino acid sequence for the residues 1–292 of the nine-haem cytochrome *c* from *D.desulfuricans* ATCC 27774. The *boxed regions* denote the haem binding regions as well as the second axial ligand (His) of the haem Fe atoms. The *grey shaded region* represents the previously known N-terminal 39 amino acid sequence and the *light blue shaded region* denotes the 253 amino acid sequence previously determined from electron density maps at 1.8 Å resolution. Within this shaded region, the *residues in red* are those which were incorrectly assigned from the 1.8 Å electron density maps in terms of side-chain shape, while those in *green* were incorrectly assigned in terms of the choice between the possible amino acid residues with similar electron density shapes

Structure analysis

The model was analysed with PROCHECK [30] and both molecules had stereochemical quality parameters

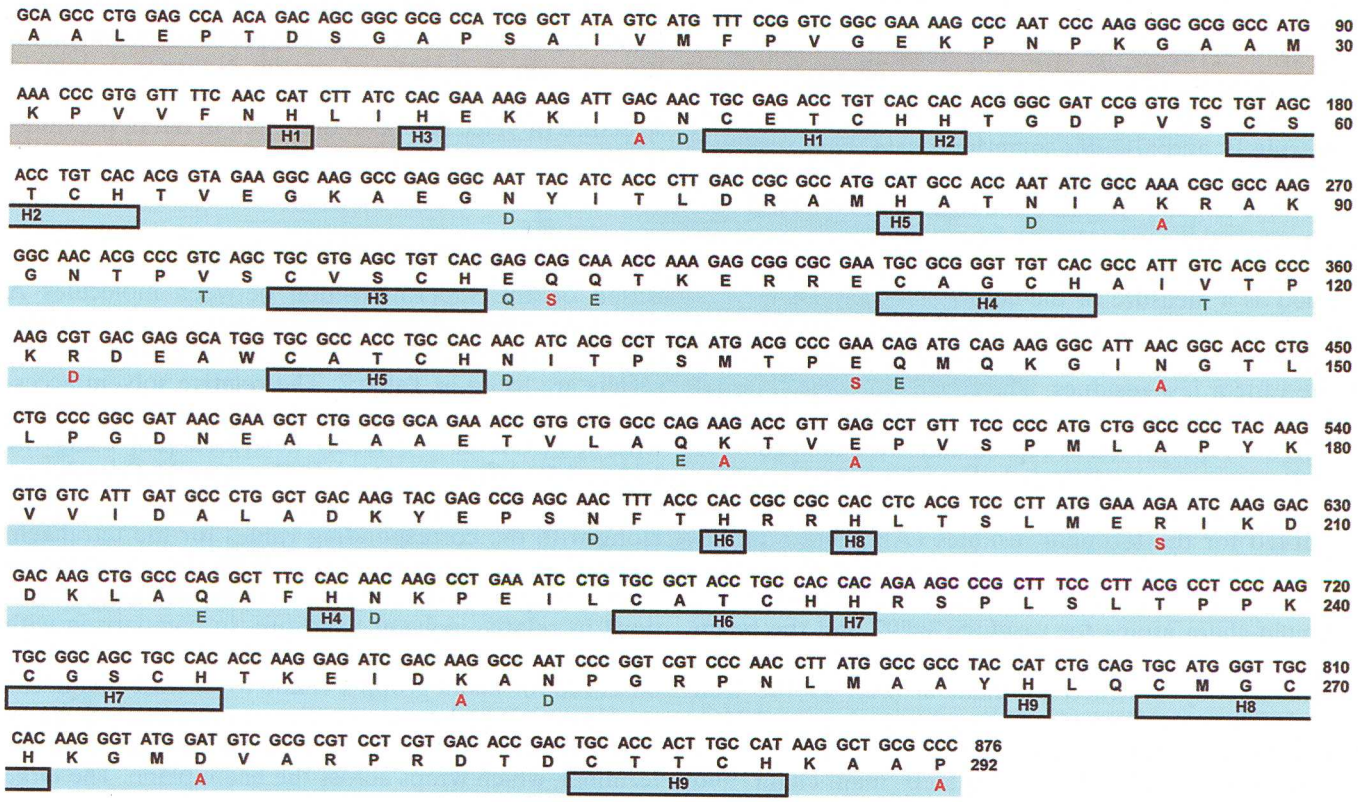

within their respective confidence intervals. The φ,ϕ plots for the non-proline and non-glycine residues are shown in Fig. 2, and only Asp188 in both molecules lies outside the normally allowed regions. This residue is located at the start of a three-residue β-turn which also includes Lys189 and Tyr190. However, a presumed hydrogen bond between D188 N and Y190 O (actual distance ca. 3.5 Å) was disrupted by the intrusion of the carboxylate group from propionate A in haem 9, where O^{1A} establishes a hydrogen bond with K189 N and O^{2A} is hydrogen-bonded to D188 N and Y190 N. This seems to strain the conformation of these three residues, Asp188 being the most affected. Overall, 87.1% of the non-proline and non-glycine residues lie within the most favoured regions. The φ,ϕ plots for proline and glycine residues (not shown) indicate that only Pro56 in molecule B adopts a conformation slightly outside the most favoured region. The φ,ϕ conformational change between Pro56A and Pro56B is not large; however, its direction is such that Pro56B is driven towards a less favoured region. This seems to be caused by a combination of two factors: on the one hand, while P56A O establishes a hydrogen bond with R198A $N^{\eta 1}$ from a symmetry related molecule, this hydrogen bond is absent in P56B; on the other hand, the side chain conformation of D55 differs between molecule A and molecule B – this is due to the intrusion of W546 between D55B $O^{\delta 2}$ and T53B $O^{\gamma 1}$, which are directly hydrogen-bonded in molecule A. Both molecules of 9Hcc in the asymmetric unit were assigned a *G*-factor of 0.0 and to (1 1 2) classes as defined by Morris et al. [31]. In both molecules, Pro279 has a *cis*-peptide bond. A multi-model Ramachandran plot [32] was calculated with SHELXL [11] in order to assess the conformational similarity between the two independent molecules in the asymmetric unit (not shown). A few residues show large conformational changes between molecule A and molecule B, and in order to better locate these residues an angular deviation plot is represented in Fig. 2c, where the angular length of the segment connecting the pairs of residues in the multi-model Ramachandran plot was calculated as $(\Delta\varphi^2+\Delta\phi^2)^{1/2}$ and can be regarded as a measure of the conformational change between equivalent residues. While most changes are smaller than 10°, variations greater than 30° are observed for a few residues. The mean isotropic thermal motion parameters for main-chain and side-chain atoms are represented in Fig. 3a and b for molecules A and B, respectively, as a function of residue number. The largest main-chain values (greater then 40 $Å^2$) are observed for the terminal residues (Ala1 and Ala292) and also for Lys90, located in a surface loop. Molecules A and B were superimposed with X-PLOR [33] using all main-chain atoms for residues 3–292 and the haem ring atoms (i.e., the four pyrrole-ring atoms and all atoms directly attached to them as well as the iron atom). The overall r.m.s. values obtained were 0.34 Å and 0.83 Å for the protein main-chain and side-chain atoms, respectively. The calculated main-chain and side-chain r.m.s. deviations between corresponding residues are included in Fig. 3c. The largest main-chain and side-chain deviations (r.m.s. values greater than 1 Å and 2 Å, respectively) occur for only a few surface residues. These deviations can be attributed to different hydrogen bonding patterns to the ordered solvent layer or to different intermolecular contacts in the crystal structure, which impose side-chain conformation adjustments in order to avoid unfavourable van der Waals contacts, and may also result in main-chain shifts. Some of these effects may also explain the conformational changes greater than 30° between equivalent residues in molecules A and B as mentioned above.

Model description

The C^{α} trace of the three-dimensional structure of 9Hcc and its haem numbering scheme are represented in Fig. 4. The haem groups are numbered according to their order of bonding to the polypeptide chain through a cysteine. The model contains 292 residues and nine haem groups, and there are two molecules in the asymmetric unit, related by a non-crystallographic twofold rotation axis approximately perpendicular to the crystallographic twofold (*b*) axis. This improved model corresponds to a molecular mass of 37.3 kDa, in close agreement with the experimentally observed value of 37.8 kDa [6]. The secondary structure of both independent molecules in the crystal structure is the same, and was analysed with PROCHECK according to the Kabsch and Sander algorithm [34]. There are no significant changes from the previously reported results [6]. The 9Hcc molecule is constituted by two domains connected by a 34-residue-long polypeptide segment. The first domain is designated as the N-terminal domain and the second as the C-terminal domain. The domain structure of 9Hcc has been discussed in detail previously [6].

Haem group geometry and environment

Based on the superimposition between molecules A and B described above, we calculated the r.m.s. deviations between the corresponding haem groups and the results are listed in Table 2. The relative solvent accessibilities of the haem groups in 9Hcc were calculated with X-PLOR as previously described [22] using the Lee and Richards algorithm [35] and an H_2O probe radius of 1.6 Å. These results are included in Table 2 along with the corresponding values for the tetrahaem cytochrome c_3 for comparison. With the exception of haem groups 2 and 5, all others show important variations in relative solvent exposure, in comparison with the corresponding haem groups of c_3 *Dd.* The increase observed for haem group 1 is due to the fact that in the tetrahaem cytochrome c_3 the corresponding haem group is more buried owing to the influence of the N-terminal, which wraps across the haem plane. The large

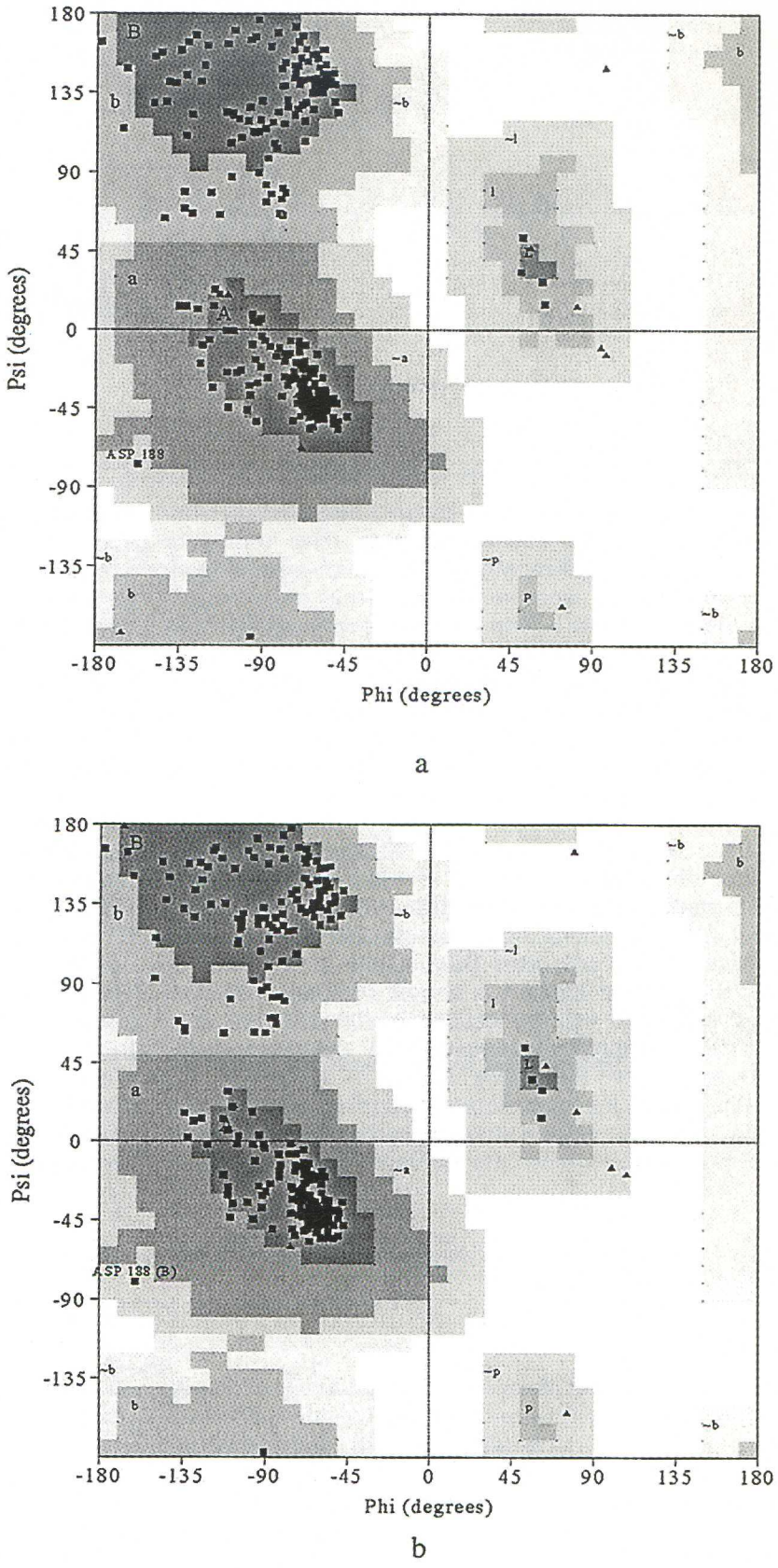

Fig. 2 **a** PROCHECK [30] φ,ϕ plot for 9Hcc molecule A; **b** PROCHECK [30] φ,ϕ plot for 9Hcc molecule B

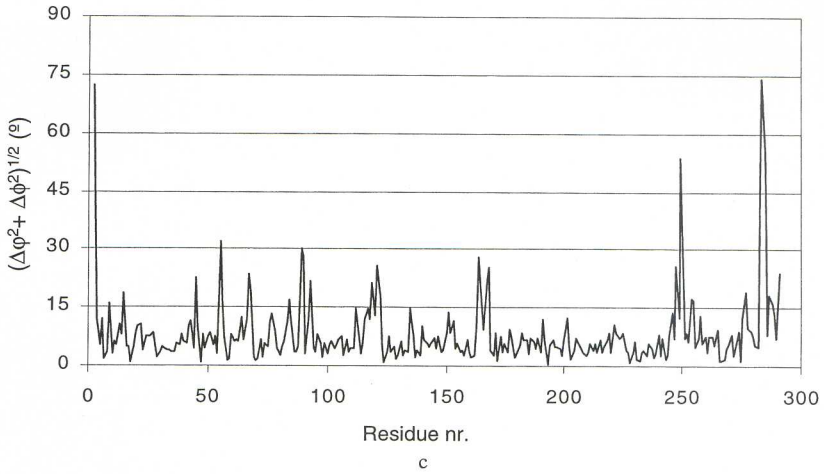

Fig. 2 c $(\Delta\varphi^2+\Delta\phi^2)^{1/2}$ angular distance plot between NCS-related residues in 9Hcc

decrease observed for haem group 3 and a smaller decrease observed for haem group 6 in 9Hcc both stem from the fact that these are closest to the isolated haem and thus become more internal, and thus more buried. On the other hand, a loop containing residues 69–78 in the tetrahaem cytochrome c_3, which interrupts an α-helix and partly covers haem group 2 (of c_3 *Dd*), is non-existent in 9Hcc, where the corresponding helix is unbroken. As a result, haem group 7 becomes considerably more exposed. The significant reduction in the relative solvent exposure of haem 8 in 9Hcc is caused by the insertion containing the second axial His ligand of isolated haem 4, absent in c_3 *Dd*. Finally, the small decrease observed for haem 9 of 9Hcc results from a slight shift towards the haem surface of the initial structural motif containing a short two-stranded anti-parallel β-sheet. Unlike any other haem group in 9Hcc and c_3 *Dd*, the isolated haem 4 is almost completely buried. This, combined with its location in the structure, suggests that it may be connected with electron transfer between the two tetrahaem clusters.

An interesting observation regarding some of the haem groups in 9Hcc is that the carboxylate groups of the propionate chains are bridged by a hydrogen-bonded water molecule, in the case of haem groups 4, 5, 7 and 9, while in haem 8 this bridge is constituted by two water molecules. It is remarkable that none of these carboxylate groups belong to a haem in the N-terminal c_3-like region. Also, the observed hydrogen bond in both 9Hcc molecules between haem 4 O^{2A} and Glu102 $O^{\varepsilon 2}$ is a clear indication that one of these residues is protonated.

The hydrogen bonding scheme involving $N^{\delta 1}$ of the histidine axial haem ligands is shown in Table 3. In c_3 *Dd*, three of the hydrogen bonds involve co-crystallized water molecules, a feature which is common in all known cytochrome c_3 structures [22]. However, in both tetrahaem clusters of 9Hcc, only one of these water molecules (W144 in molecule A and W540 in molecule B) is conserved and the overall pattern is quite different. While in c_3 *Dd* all the other hydrogen bond acceptors are main-chain carbonyl oxygens, in 9Hcc there are also two instances where the hydrogen bond is established with a side-chain oxygen (Glu41 $O^{\varepsilon 1}$ near haem 1 and Thr196 $O^{\gamma 1}$ near haem 8). Also, near haem 9, His288 $N^{\delta 1}$ is hydrogen bonded with its own carbonyl oxygen, which is unprecedented for a c_3 or c_3-like cytochrome. This may be due to the relative orientation

Table 2 Average *B* values, relative solvent exposure (RSE) (%) and r.m.s. differences for the haem groups in molecules A and B of 9Hcc from *Dd* 27774

Haem	Average *B* (Å^2)		% RSE			r.m.s.d. (Å)		
	9Hcc A	9Hcc B	9Hcc A	9Hcc B	c_3*Dd*	Total	Ring[a]	Non-ring
1	14.4	21.1	14.3	15.9	10.9	0.21	0.16	0.35
2	17.9	19.8	12.8	15.5	13.1	0.22	0.12	0.45
3	12.5	17.9	2.5	2.2	18.0	0.16	0.12	0.27
4	11.4	15.9	0.2	0.3	–	0.11	0.09	0.16
5	13.0	12.9	13.3	14.0	12.8	0.09	0.09	0.11
6	12.5	17.2	8.5	8.5	10.9	0.24	0.13	0.48
7	13.3	19.0	21.3	20.9	13.1	0.31	0.20	0.58
8	15.7	21.3	9.0	12.0	18.0	0.39	0.19	0.82
9	13.4	18.4	10.8	10.4	12.8	0.25	0.25	0.20

[a]The haem ring includes the four pyrrole-ring atoms and all atoms directly attached to them

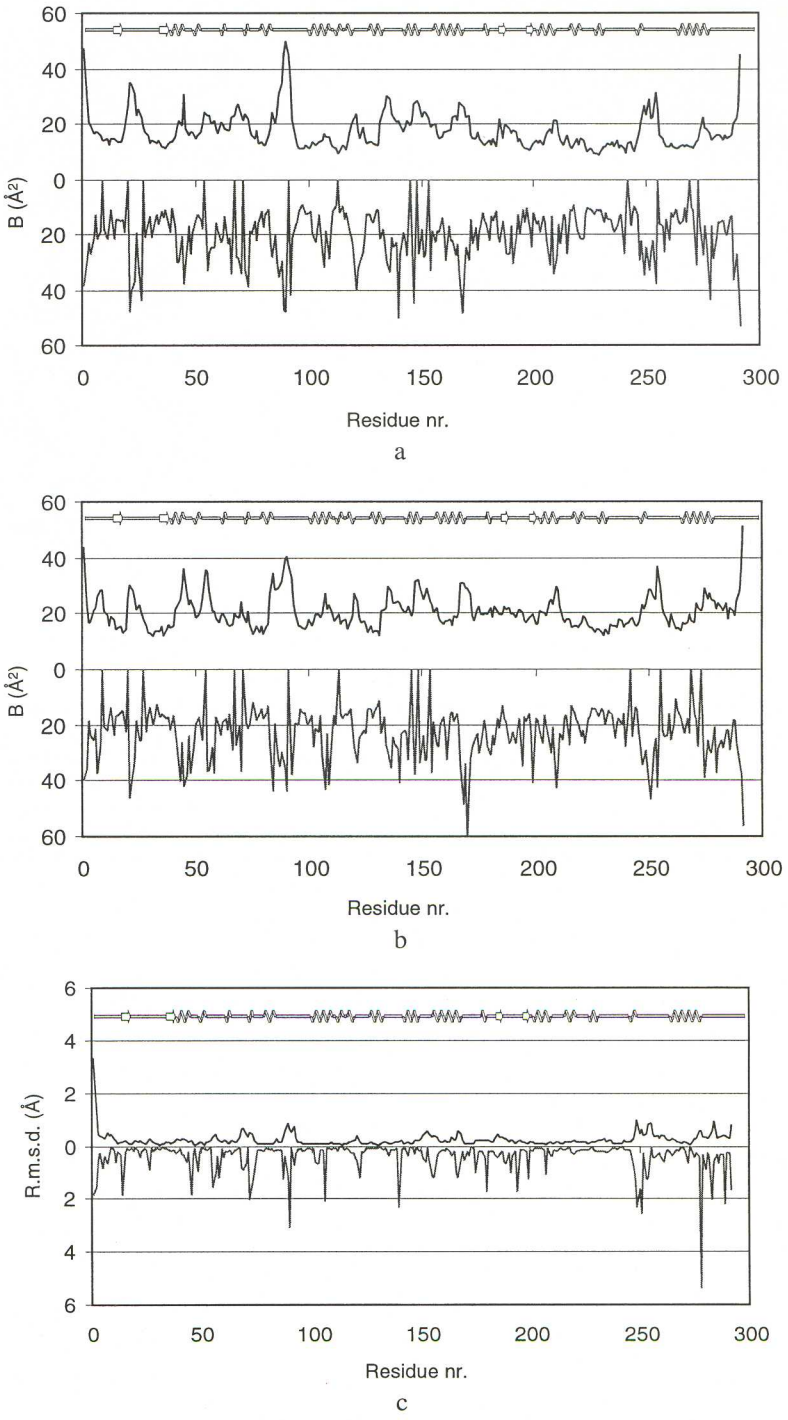

Fig. 3 **a** Main-chain (above *x*-axis) and side-chain (below *x*-axis) average *B*-factor (Å^2) plotted as a function of residue number for the protein chain of 9Hcc A; **b** main-chain (above *x*-axis) and side-chain (below *x*-axis) average *B*-factor (Å^2) plotted as a function of residue number for the protein chain of 9Hcc B; **c** main-chain (above *x*-axis) and side-chain (below *x*-axis) r.m.s. deviations between the protein chains of 9Hcc molecules A and B; overlaid on these plots is a PROCHECK [30] linear diagram of the 9Hcc secondary structure according to Kabsch and Sander [34]

of the His288 side chain to Cys284, the first residue in the haem 9 binding motif, combined with the proximity of Tyr190, which not only blocks the solvent access to His 288 but also probably restricts the internal cavity volume below the threshold needed to accommodate a co-crystallized water molecule. The angles between the planes of the imidazole rings of the histidine axial haem ligands are also considered significant structural parameters. These angles are listed in Table 4 and were estimated as the arithmetic mean of the two dihedral angles $C^{\varepsilon 1}$–$N^{\varepsilon 2}$···$N^{\varepsilon 2}$–$C^{\varepsilon 1}$ and $C^{\delta 2}$–$N^{\varepsilon 2}$···$N^{\varepsilon 2}$–$C^{\delta 2}$. All the interplanar angles are different in 9Hcc and in c_3 *Dd*. Inspection of the superimposed three-dimensional structures reveals that, for most cases, one of the histidine imidazole rings in 9Hcc is roughly parallel with its counterpart in c_3 *Dd*, while the second imidazole ring is in a different orientation relative to the first. Moreover, significant differences exist also between the N-terminal and C-terminal c_3-like regions in 9Hcc. The angles between the planes of the imidazole rings of the histid-

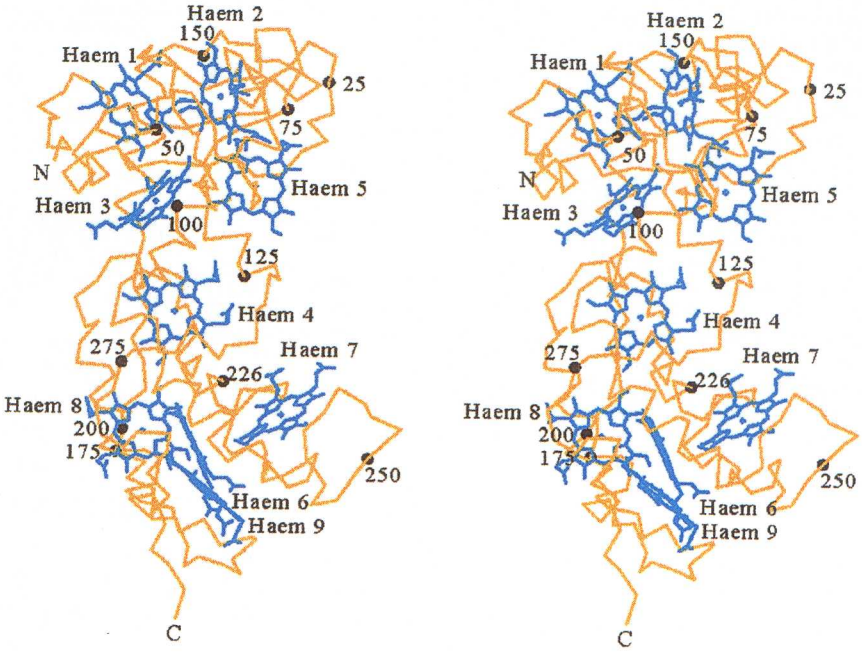

Fig. 4 Stereoview of the C^{α} trace and haem group numbering for the three-dimensional structure of 9Hcc. Pictures drawn with MOLSCRIPT [39]

Table 3 Hydrogen bonds and interplanar angles involving ligated histidines in 9Hcc

Haem 9Hcc	Donor atom	Hydrogen bond distance $N^{\delta 1}$...donor (Å)		Comparison with c_3 *Dd*[a]		
		9Hcc A	9Hcc B			Haem c_3 *Dd*
1						1
His 37	$O^{\varepsilon 1}$ (Glu41)	2.78	2.72	w	His22	
His51	O (W144; W540)	2.83	2.84	w	His34	
2						2
His52	O (W290; W555)	2.80	2.85	m	His35	
His63	O (Ile74)	2.97	2.83	m	His52	
3						3
His40	O (Asn36)	2.87	2.88	m	His25	
His101	O (W15; W448)	2.88	2.95	m	His83	
4						–
His115	O (W174; W782)	3.13	2.92		–	
His218	O (W218; W482)	2.92	2.71		–	
5						4
His81	O (Asp77)	2.68	2.70	m	His69	
His131	O (Lys31)	2.70	2.67	w	His106	
6						1
His197	O (W12; W473)	2.99	3.10	w	His22	
His229	O (W2; W468)	2.89	2.88	w	His34	
7						2
His230	O (W60; W466)	2.85	2.91	m	His35	
His245	O (Pro257)	2.83	2.95	m	His52	
8						3
His200	$O^{\gamma 1}$ (Thr196)	2.87	2.93	m	His25	
His271	O (W214; W489)	2.89	2.89	m	His83	
9						4
His264	O (W166; Ac5)	2.83	2.75	m	His69	
His288	O (His288)	2.71	2.82	w	His106	

[a] w, His $N^{\delta 1}$ hydrogen bonds to a water molecule; m, His $N^{\delta 1}$ hydrogen bonds to a main-chain carbonyl oxygen

ines attached to haem groups 1 and 6 have similar interplanar angles, as do those linked to haem groups 3 and 8. However, the planes of the imidazole rings of the histinines coordinating haems 2 and 7, as well as 5 and 9, have radically different angles, not only in terms of magnitude but also in terms of orientation as given by the sign of the angle, as discussed above. These differences can largely be attributed to the differences in the the hydrogen-bonding pattern of the $N^{\delta 1}$ atoms of the histidine axial haem ligands, also discussed above.

Table 4 Interplanar angles (°) involving ligated histidines in 9Hcc and c_3 *Dd*[a,b]

N-terminal c_3-like region			C-terminal c_3-like region			c_3 *Dd*	
Haem	9Hcc A	9Hcc B	Haem	9Hcc A	9Hcc B	Haem	
1	−152.4	−153.1	6	−149.0	−146.4	1	−6.5
2	36.8	39.3	7	−56.2	−60.7	2	−110.1
3	25.2	25.1	8	25.5	25.7	3	3.3
4	−171.4	−173.6	–	–	–	–	–
5	−25.2	−23.6	9	46.9	38.2	4	4.3

[a] Absolute values close to 0° indicate that the equivalent $C^{\varepsilon 1}$ or $C^{\delta 2}$ atoms in the neighbouring axial His residues tend to be eclipsed, while absolute values close to 180° indicate that the $C^{\varepsilon 1}$ atoms of one His residue tend to eclipse the $C^{\delta 2}$ atoms of the second residue and vice versa

[b] The sign of this angle also provides some information: taking any one of the His planes as reference, and looking down the direction defined by the two $N^{\varepsilon 2}$ atoms, positive values mean that the second plane is twisted counter-clockwise and vice versa for the negative values

Electron transfer properties of 9Hcc

In order to characterize the molecular surface of this molecule, two properties were mapped on it (Fig. 5): the electrostatic potential, calculated using GRASP (with the GROMOS charge set) and the electron transfer decay coupling from any haem to any specific point at the surface. This mapping is meant to characterize the surface properties in terms of electrostatic interactions relevant to association with other proteins and, at the same time, to provide a qualitative idea of the electron transfer propensities of these same surface zones. Overall, the surface of the 9Hcc molecule shows mainly negative potentials, especially in the N-terminal domain. However, there are small regions where positive potentials are evident. The region near haem 4 is one of these, but the zone with the highest positive character in the molecule includes haems 6 and 8 along with their immediate surroundings. This strong positive character is due to patches of lysine and arginine residues: Arg278, Lys180, Arg198, Arg199, Arg207 and Arg109.

The electron transfer characteristics of the surface show some interesting features. The surface of the C-terminal domain and around the isolated haem 4 displays large decay coupling values, an indication that, in the absence of other controlling factors, molecular associations with this region will have a large probability of electron transfer. In contrast, in the N-terminal domain, only the exposed parts of the haem group surfaces seem to display high decay coupling values. This is most evident in the case of haem groups 1 and 2. Therefore, electron transfer in this part of the molecule should be more specific, requiring particular modes of molecular association.

Electron transfer between the nine haems of the molecule seems to be organized into two interacting domains. Electron transfer calculations between all haem groups in the molecule show that electron transfer is comparable within each of the two tetrahaem clusters, as well as between these clusters and the isolated haem 4 (see Fig. 6), which appears to function as an inter-cluster bridge. Therefore, electron transfer within the molecule should be fast. This hypothesis is valid in the absence of other electron transfer controlling factors, within the framework of the Pathways model.

Modelling of the interaction between 9Hcc and the tetrahaem cytochrome c_3 in *Dd* 27774

With the aim of understanding the molecular association and electron transfer experimentally observed between 9Hcc and the tetrahaem cytochrome c_3 in *Dd* 27774 [6], we performed docking simulations of these two molecules, as described in Materials and methods. Two hundred docking simulations were calculated and the final annealed solutions cluster as shown in Fig. 7. Ninety seven different clusters were found, which can be ranked by their interaction energy. A large number of solutions are observed, but their interaction energies are quite different. Some are probably not very significant, given their large energy difference from the best solution. The best solution has a substantially lower energy than the second best (–248.2 kJ/mol for the best and –238.1 kJ/mol for the second best). Figure 8 contains a representation of the interaction solutions of tetrahaem cytochrome c_3 with 9Hcc, by depicting the centre of geometry of the small molecule final positions as spheres around the large molecule. The 10 best clusters are coloured red and in fact correspond to 52 docking solutions (i.e. 26% of the solutions). The best solutions tend to cluster in specific places of the molecule, mostly in the N-terminal domain around haems 1 and 2. Indeed, the solutions included in the 10 best ranks correspond to interactions between the haem 4 region of the tetrahaem cytochrome c_3 and the haem 1 and 2 regions of 9Hcc. In this group, only rank 10 does not correspond to a direct interaction between haem groups from the two proteins. Ranks 1 and 2 correspond to a direct interaction with haem 2 of 9Hcc.

The results obtained here can be interpreted as possible solutions of the molecular interaction between the two proteins. This means that one should not focus on only one solution to explain the electron transfer because the interaction energy function used here is a crude approximation for the molecular interactions that are expected to occur in solution. Besides these modell-

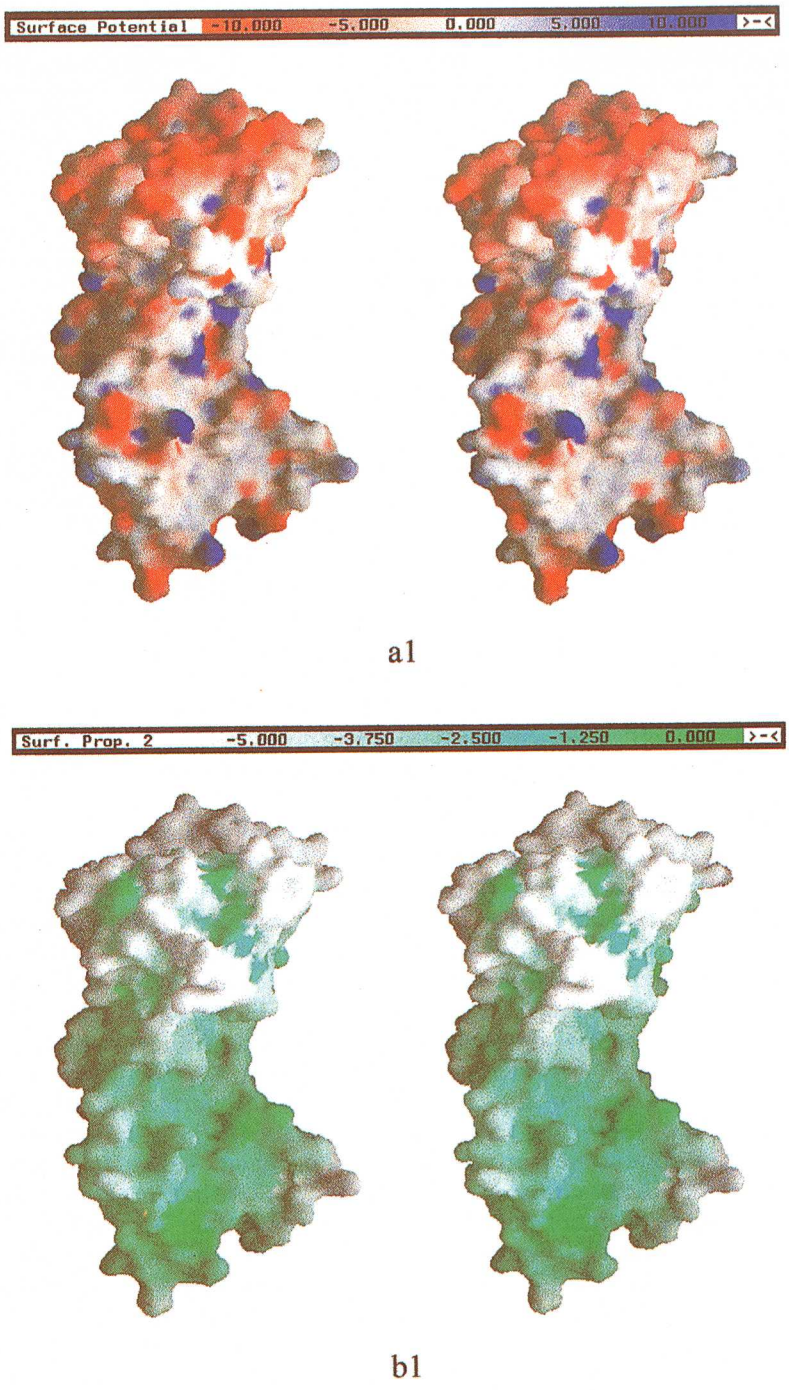

Fig. 5 Stereo representations of the surface characteristics of the 9Hcc in two configurations. The molecular orientation in (a1, b1) is similar to that of Fig. 4, and in (a2, b2) is rotated by 180° relative to (a1, b1). **a** Electrostatic potential mapping at the molecular surface. *Red coloured zones* correspond to negative potentials, while *blue coloured zones* correspond to positive potentials. The range of potential spans from –10 to $10kT/e$. **b** Electron transfer decay coupling mapping at the molecular surface. *Green coloured zones* correspond to high coupling values for electron transfer from the donor center. The range spans from –5 to 0 (in $\log_{10}[(\text{decay})^2]$ units as obtained from GREENPATH [20]). The coupling values correspond to the sum of decay couplings from all haem groups to any given point at the surface, i.e. all haems are considered as donors

ing issues, one should also consider that electron transfer between redox proteins may not necessarily occur through the formation of one specific complex, but rather through multiple possible associations with differing electron transfer capabilities [36], or through reorganization (conformational change) between different complexes [19]. In any case, the results presented here suggest a trend for the interaction between these two molecules: haem 4 of cytochrome c_3 interacts preferentially with either haem 2 or haem 1 of 9Hcc.

To further characterize the associations mentioned above, we optimized the structure of the three best complexes using molecular dynamics simulations, in order to model the close association between the two molecules prior to electron transfer. This is important because the rigid complex solutions found with the structures of the isolated proteins can substantially change when the molecules are brought together [19, 23]. The two best complex solutions are associations between haem 4 of cytochrome c_3 and haem 2 of 9Hcc, related by a 180° rotation of the c_3 molecule about an axis approximately defined by its haem 4 and haem 1

Fig. 5 Continued

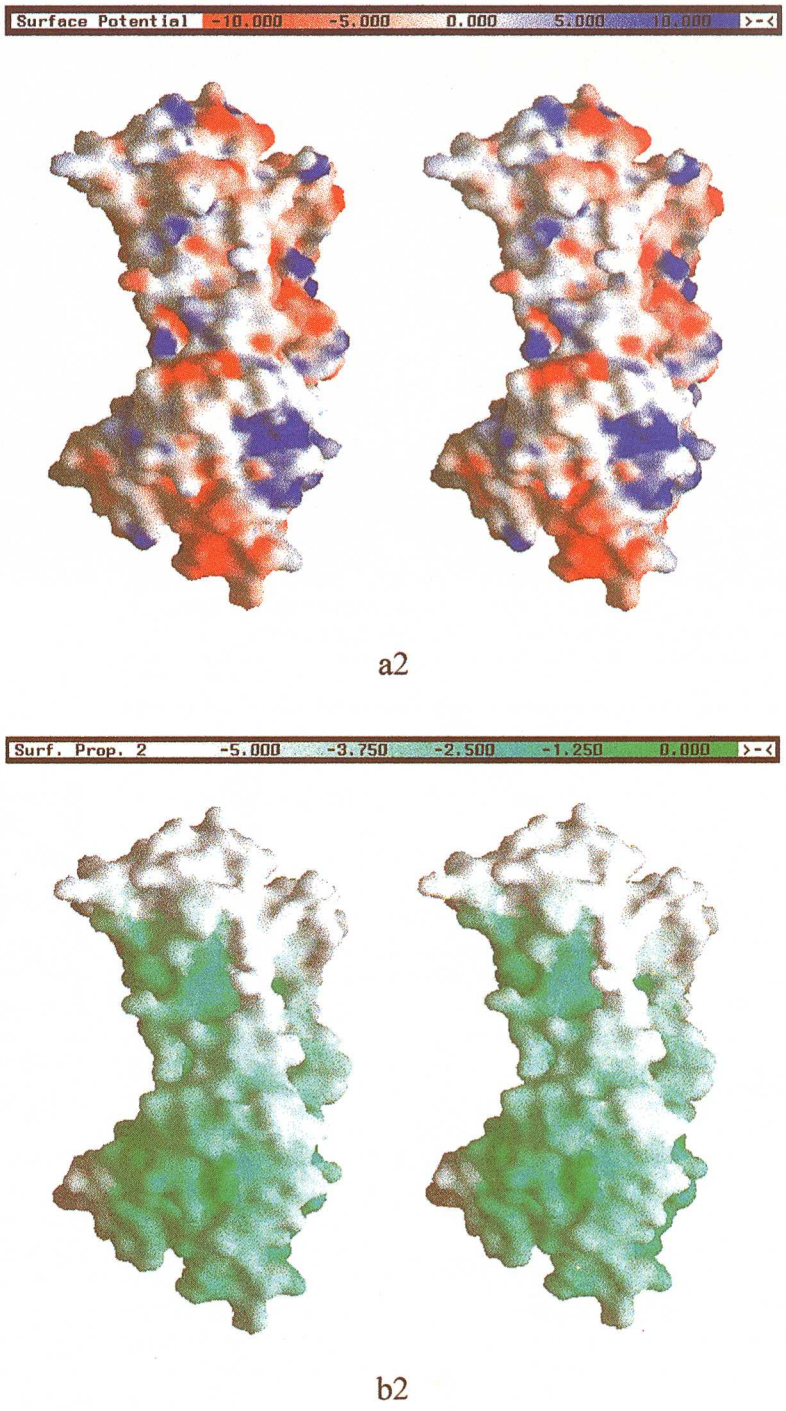

groups. The third solution corresponds to the interaction between haem 4 of cytochrome c_3 and haem 1 of 9Hcc. The results of the molecular dynamics are presented in Fig. 9. The molecular dynamics refinement led to significant changes in the interaction between the two proteins, reducing in all cases the distance between haem groups. In the first case, the haem groups brought into contact are parallel to each other but slightly shifted. In the second solution the haems are on top of each other, but twisted by approximately 45°. In the third solution, the haems are parallel and aligned with each other. Table 5 lists the charged groups that are placed into contact in the three associations studied here. As can be seen, there are a variety of charged groups that are brought into contact by the interaction between the two cytochromes. These groups are in general, as expected, negatively charged groups from 9Hcc and positively charged ones from cytochrome c_3. In the case of the third solution this behaviour is less marked, since cytochrome c_3 contributes with three negatively

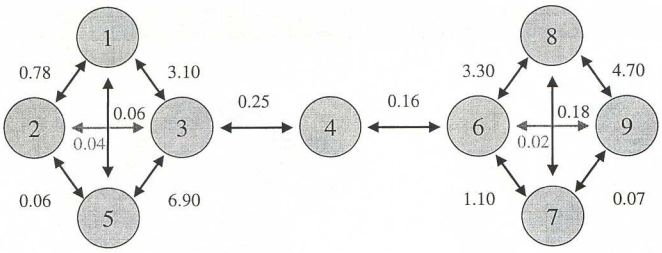

Fig. 6 Simplified electron transfer paths within 9Hcc and their respective decay coupling factors, multiplied by 1,000. These numbers correspond to a calculation without crystallographic water molecules. However, when water molecules are included, the results do not change for the paths represented in the figure, indicating that the best electron transfer paths do not follow through water molecules

Table 5 Charged groups that interact in the different docking solutions after molecular dynamics and energy minimization. The table contains also some interactions with polar groups when the other group is a charged group. The interactions presented here do not all fulfill the criteria for the establishment of a hydrogen bond, but are rather based on electrostatic proximity

	9Hcc	c_3 Dd
Docking 1	Gly20 (C=O)	Lys102
	Glu21 (C=O)	Lys102
	Glu48	Lys59
	Asp55	Tyr65
	Lys68	C-terminal
	Glu70	Lys16
	Glu70	His106[a]
	Glu70	Haem 4[b]
	Ile146 (C=O)	Lys102
	Haem 1 (propionate A)	Lys71
	Haem 1 (propionate A)	Lys94
Docking 2	Glu21	Lys59
	Glu48	Lys102
	Glu70	His69[a]
	Glu70	Haem 4[b]
	Gly128 (C=O)	Lys58
	Haem 2 (propionate D)	Lys71
	Haem 2 (propionate D)	Lys94
Docking 3	N-terminal	Glu73
	Glu4	Lys59
	Asp7	Lys59
	Glu21 (C=O)	Lys59
	Glu21	Lys90
	Asp45	Lys58
	Asp55	Cys100 (NH)
	Lys68	Glu92
	Glu70	Lys95
	Lys144	Glu89
	Haem 1 (propionate A)	Thr98
	Haem 1 (propionate A)	Lys71
	Haem 1 (propionate A)	Lys94
	Haem 1 (propionate D)	Lys94

[a] Axial histidine of haem 4
[b] Interacts with the haem plane

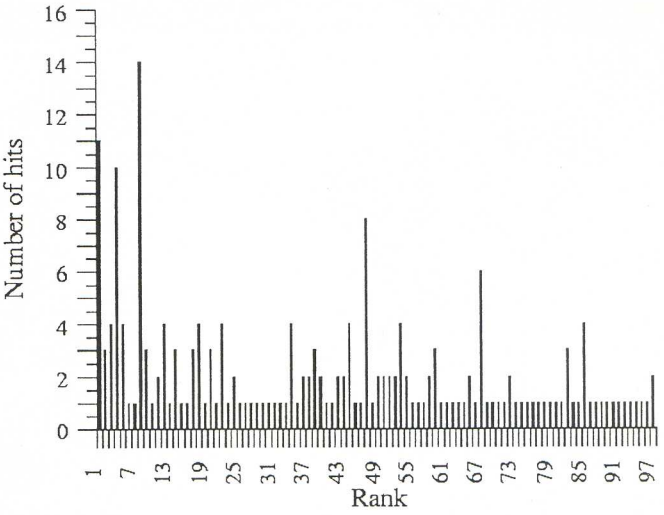

a

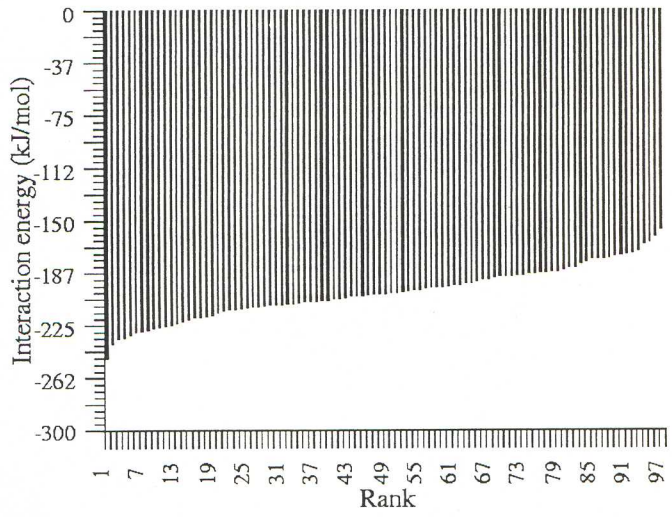

b

Fig. 7 Results from the 200 docking simulations. **a** Number of hits for each rank; conformations were clustered using a r.m.s. deviation tolerance of 1.0 Å. **b** Minimum interaction energy for the members of each rank

charged groups that interact with three positively charged groups of 9Hcc.

There are two residues from 9Hcc, Glu21 and Glu70 that interact with cytochrome c_3 in all three solutions analysed here. These are close together and at the edge of the contact zone between the two molecules. From the cytochrome c_3 side, there are three lysines, Lys59, Lys71 and Lys94, that interact with 9Hcc in all three docking solutions. Similarly to the acids of 9Hcc, these lysines are at the edge of the contact zone between the two proteins. The three lysines are located in the long, predominantly helical, region that binds haem III of cytochrome c_3. Given the relative importance of these charged residues for both molecules in their simulated

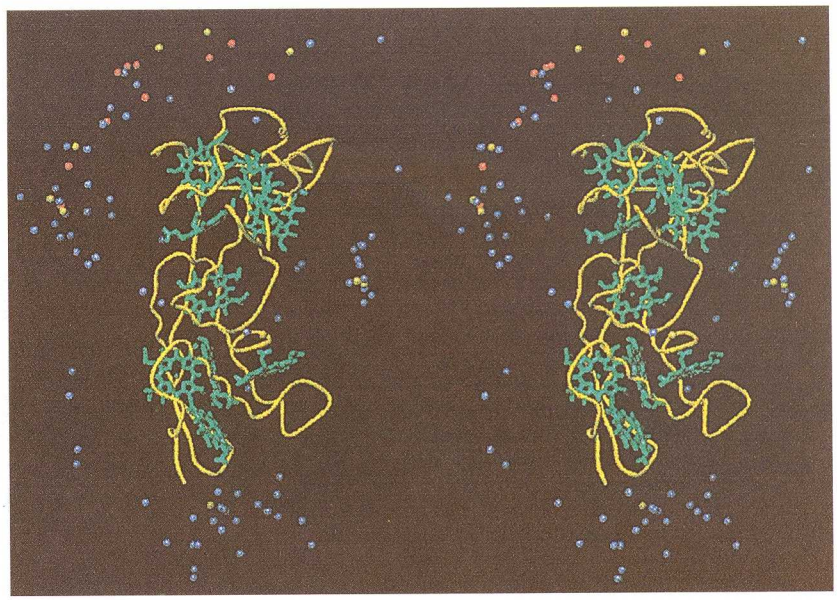

Fig. 8 Stereo representation of the centre of geometry of all 97 interaction ranks of tetrahaem cytochrome c_3 (shown as *spheres*; each cluster is represented only once, independently of the number of solutions it contains) around 9Hcc (only the protein fold and haem groups are represented). The 10 best ranks are coloured *red*; the remaining up to the 20th best are coloured *yellow* and the rest are coloured *blue*

interaction, it would be interesting to replace them by non-charged ones in order to verify their role in the molecular association and subsequent electron transfer.

Electron transfer calculations on the final complexes, between haem 4 of cytochrome c_3 and haem 2 (for ranks 1 and 2) or haem 1 (for rank 3) of 9Hcc, indicate that the best paths are always for direct electron transfer between the haem groups, and the decay coupling values (T_{DA}) (Table 6) are as high as intramolecular electron transfer within the tetrahaem clusters of 9Hcc. In the absence of other controlling factors, this result is an indication of high electron transfer between the two proteins.

Conclusion

The three-dimensional structure of the nine-haem cytochrome *c* from *D. desulfuricans* ATCC 27774 highlights the success of the tetrahaem structural arrangement, a motif found very frequent in *Desulfovibrio* organisms (the archetypal case being the cytochrome c_3) as a highly adaptable framework and building block for more complex molecules. The three-dimensional stuctures of two di-tetrahaem cytochromes c_3 from *D. norvegicum* [40] and *D. gigas* [41], formed by the association of two separate tetrahaem c_3 units, were already an example of this trend. The cytochrome 9Hcc is the first known three-dimensional structure where multiple copies of a tetrahaem cytochrome c_3-like fold are present in the same polypeptide chain. The structures of the 16-haem high-molecular-weight cytochrome (Hmc) isolated from *D. vulgaris* (strains Miyazaki and Hildenborough) and *D. gigas* were predicted to be formed by the association of three tetrahaem, one trihaem and one single haem motifs [42–44]. In view of the high sequence homology of the C-terminal 285 residues of the Hmc from *D. vulgaris* Hildenborough with the 9Hcc, the structure of the latter provides a glimpse, albeit incomplete, into the three-dimensional structures of these Hmc molecules [6]. All these studies seem to indicate an evolutionary trend based on the tetrahaem common motif.

We suggest in this work a possible molecular basis for the electron transfer interaction observed in vitro between the tetrahaem cytochrome c_3 and the nine-haem cytochrome *c* from Dd 27774 [6]. The electron transfer characteristics of the molecular surface of the 9Hcc C-terminal domain would indicate a non-specific electron transfer, given that the exposed portions of the haem groups constitute a large fraction of this molecular surface and there are also many short electron transfer paths between the surface residues and the haems. However, these electron transfer characteristics alone cannot be taken as the driving force towards a physical interaction between two molecules. Our docking studies, on the other hand, contain reasonable physical descriptions for molecular interactions, and suggest that the interaction between these two cytochromes is very specific. Contrary to the situation in the C-terminal domain, in the N-terminal region there are very well-defined surface patches with favourable electron transfer characteristics. The most probable dock-

Table 6 Best paths for electron transfer after molecular dynamics refinement and their decay coupling values (T_{DA}). The protein atoms indicated are those participating in the bridging orbital

Rank	Path		T_{DA}
	From (c_3 *Dd* atom)	To (9Hcc atom)	
1	haem 4 C^{MB}	haem 2 C^{AC}	4.0×10^{-3}
2	haem 4 C^{BB}	haem 2 C^{BC}	2.5×10^{-3}
3	haem 4 C^{BB}	haem 1 C^{HB}	3.6×10^{-3}

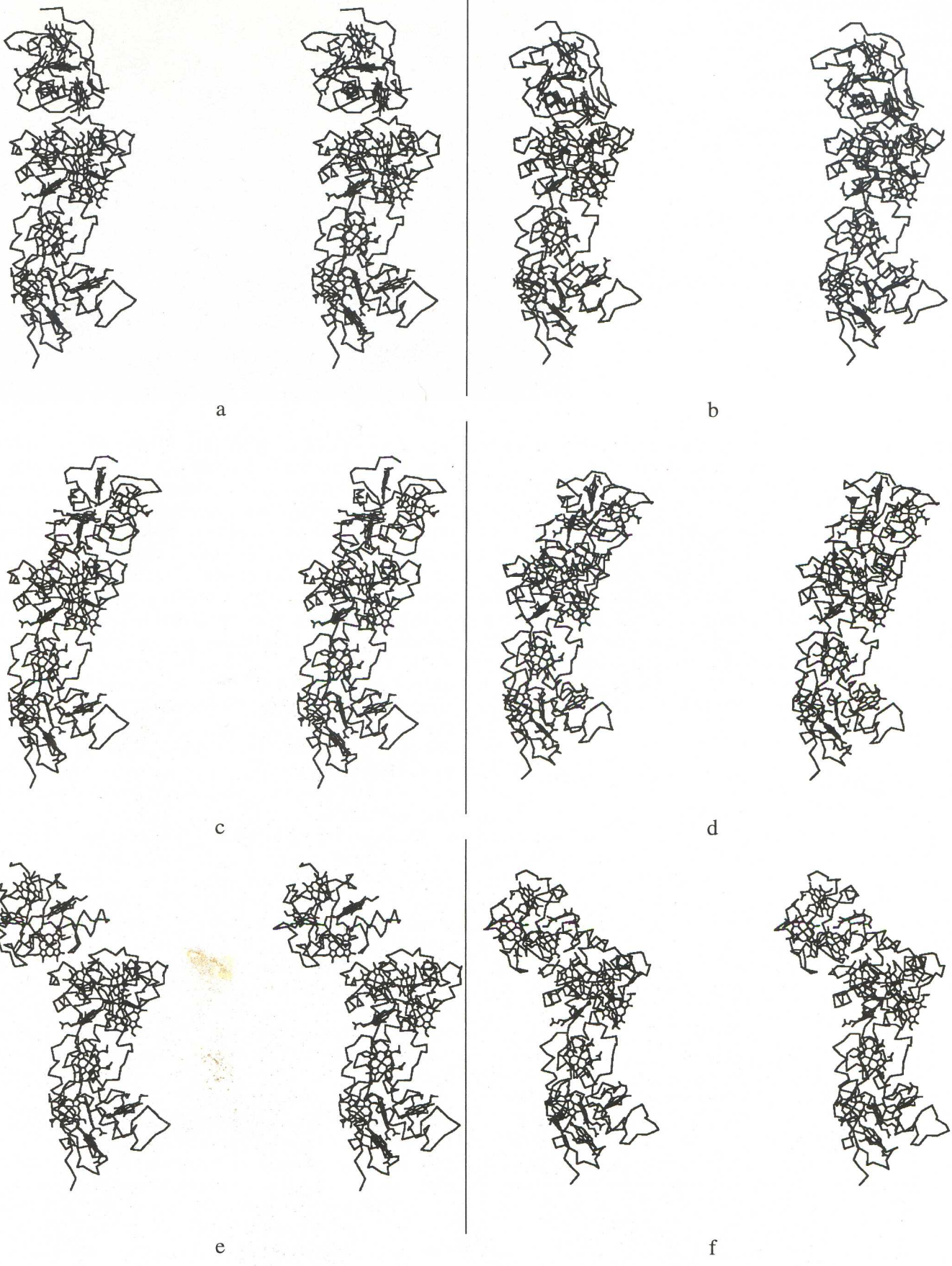
a
b
c
d
e
f

Fig. 9 Stereo representations for the three best ranks for the interaction between the tetrahaem cytochrome c_3 and 9Hcc, before and after molecular dynamics refinement. Only the protein C^{α} atoms and the haem groups are represented. **a** Rank 1, before MD; **b** rank 1, after MD; **c** rank 2, before MD; **d** rank 2, after MD; **e** rank 3, before MD; **f** rank 3, after MD

ing solutions place haem 4 of the tetrahaem cytochrome c_3 in contact with either one of these patches, which correspond to the exposed surfaces of haem groups 1 and 2 of 9Hcc. This may result from a favourable electrostatic complementarity between the positively charged surface region around haem 4 of the tetrahaem cytochrome c_3 and these negatively charged regions of 9Hcc, coupled with a significant degree of surface complementarity. Therefore, the electron transfer between these two proteins does not seem to result from random interactions, but rather from specific associations, a situation which has been suggested to be characteristic of physiological electron transfer interactions [45] as opposed to non-physiological interactions [46]. It now remains to be seen if a similar situation can be found from modelling studies of the interactions between 9Hcc, flavodoxin and rubredoxin from *Dd* 27774, for which the structures are known to atomic resolution [47, 48]. It is important to note here that, whereas the tetrahaem cytochrome c_3 is found in the periplasmic space, both flavodoxin and rubredoxin are found in the bacterial cytoplasm, and it has been suggested that 9Hcc may act as a transmembrane redox carrier [6]. Thus it is crucial to determine if the specific interaction that exists between the tetrahaem cytochrome c_3 and the N-terminal domain of 9Hcc can be mirrored by a similar specific interaction between the C-terminal domain of 9Hcc and one or both of these two cytoplasmic electron carriers. Further work is in progress at our laboratories, aimed at testing this hypothesis.

Acknowledgements This work was funded by the European Union (Network CHRX-CT93-0143 and grants BIO2/CT94/2052 and BIO4/CT96/0413) and JNICT (grants PRAXIS/2/2.1/QUI/17/94 and PBIC/C/BIO/3037/95). The authors would also like to thank Júlia Lobato (Instituto Gulbenkian de Ciência) for the DNA sequencing.

References

1. Yagi T, Honya M, Tamiya N (1968) Biochim Biophys Acta 153:699–705
2. Louro RO, Catarino T, Le Gall J, Xavier AV (1997) JBIC 2:488–491
3. Pereira IAC, Teixeira M, Xavier AV (1998) Struct Bonding 91:65–89
4. Liu M-C, Costa C, Coutinho IB, Moura JJG, Moura I, Xavier AV, LeGall J (1988) J Bacteriol 170:5545–5551
5. Coelho AV, Matias PM, Sieker LC, Morais J, Carrondo MA, Lampreia J, Costa C, Moura JJG, Moura I, Le Gall J (1996) Acta Crystallogr Sect D 52:1202–1209
6. Matias PM, Coelho R, Pereira IAC, Coelho AV, Thompson AW, Sieker LC, Le Gall J, Carrondo MA (1999) Structure 7:119–130
7. Pereira IAC, Romão CV, Xavier AV, Le Gall J, Teixeira M (1998) JBIC 3:494–498
8. Starkey RL (1938) Arch Microbiol 9:268–304
9. Ausubel FM, Brent R, Kingston RE, Moore DD, Seidman JG, Smith JA, Struhl K (1995) Current protocols in molecular biology. Greene/Wiley, New York
10. Roussel A, Fontecilla-Camps JC, Cambillau C (1990) XV IUCr Congress Abstracts, Bordeaux, France, pp 66–67
11. Sheldrick GM, Schneider TR (1997) Methods Enzymol 277:319–343
12. Abola EE, Bernstein FC, Bryant SH, Koetzle TF, Weng J (1987) In: Allen FH, Bergeroff G, Sievers R (eds) Crystallographic databases – information content, software systems, scientific applications. Data Commission of The International Union of Crystallography, Bonn, pp 107–132
13. Bernstein FC, Koetzle TF, Williams GJB, Meyer EF Jr, Brice MD, Rodgers JR, Kennard O, Shimanouchi T, Tasumi M (1977) J Mol Biol 112:535–542
14. Marcus RA, Sutin N (1985) Biochim Biophys Acta 811:265–322
15. Beratan DN, Onuchic JN (1996) In: Bendall DS (ed) Protein electron transfer. BIOS, Oxford, pp 23–42
16. Beratan DN, Onuchic JN, Winkler JR, Gray HB (1992) Science 258:1740–1741
17. Betts JN, Beratan DN, Onuchic JN (1992) J Am Chem Soc 114:4043–4046
18. Frazão C, Soares CM, Carrondo MA, Pohl E, Dauter Z, Wilson KS, Hervás M, Navarro JA, De la Rosa MA, Sheldrick GM (1995) Structure 3:1159–1169
19. Ullmann GM, Knapp E-W, Kostic NM (1997)) J Am Chem Soc 119:42–52
20. Regan JJ (1994) Greenpath software v. 0.971. Jeffrey J. Regan, San Diego
21. Goodsell DS, Olson AJ (1990) Proteins 8:195–202
22. Simões P, Matias PM, Morais J, Wilson K, Dauter Z, Carrondo MA (1998) Inorg Chim Acta 273:213–224
23. Cunha CA, Romão MJ, Sadeghi SJ, Valetti F, Gilardi G, Soares CM (1999) JBIC 4:360–374
24. Mehler EL, Solmajer T (1991) Protein Eng 4:903–910
25. van Gunsteren WF, Berendsen HJC (1987) Groningen molecular simulation (GROMOS) library manual. Biomos, Groningen, The Netherlands
26. Smith LJ, Mark AE, Dobson CM, van Gunsteren WF (1995) Biochemistry 34:10918–10931
27. Martel P, Soares CM, Baptista AM, Fuxreiter M, Náray-Szabó G, Louro RO, Carrondo MA (1999) JBIC 4:73–86
28. van Gunsteren WF, Berendsen HJC (1990) Angew Chem Int Ed Engl 29:992–1023
29. Ryckaert J-P, Ciccotti G, Berendsen HJC (1977) J Comput Phys 23:327–341
30. Laskowski RA, MacArthur MW, Moss DS, Thornton JM (1993) J Appl Crystallogr 26:283–291
31. Morris AL, MacArthur MW, Hutchinson EG, Thornton JM (1992) Proteins 12:345–364
32. Kleywegt GJ (1996) Acta Crystallogr Sect D 52:842–857
33. Brünger AT (1992) X-PLOR, version 3.1:a system for X-ray crystallography and NMR. Yale University Press, New Haven
34. Kabsch W, Sander C (1983) Biopolymers 22:2577–2637
35. Lee B, Richards FM (1971) J Mol Biol 55:379–400
36. Northrup SH (1996) In: Bendall DS (ed) Protein electron transfer. BIOS, Oxford, pp 69–97
37. Collaborative Computational Project Number 4 (1994) Acta Crystallogr Sect D 50:760–763
38. Read RJ (1986) Acta Crystallogr Sect A 42:140–149
39. Kraulis PJ (1991) J Appl Crystallogr 24:946–950
40. Czjzek M, Guerlesquin F, Bruschi M, Haser R (1996) Structure 4:395–404

41. Frazão C, Sieker L, Sheldrick G, Lamzin V, Le Gall J, Carrondo MA (1999) JBIC 4:162–165
42. Higuchi Y, Inaka K, Yasuoka N, Yagi T (1987) Biochim Biophys Acta 911:341–348
43. Pollock WBR, Loutfi M, Bruschi M, Rapp-Giles BJ, Wall JD, Voordouw G (1991) J Bacteriol 173:220–228
44. Chen L, Pereira MM, Teixeira M, Xavier AV, Le Gall J (1994) FEBS Lett 347:295–299
45. Ubbink M, Ejdebäck M, Karlsson G, Bendall DS (1998) Structure 6:323–335
46. Ubbink M, Bendall DS (1997) Biochemistry 36:6326–6335
47. Romero A, Caldeira J, Le Gall J, Moura JJG, Romao MJ (1996) Eur J Biochem 239:190–196
48. Sieker LC, Stenkamp RE, Jensen LH, Prickril B, Le Gall J (1986) FEBS Lett 208:73–76